Evaluation of ^{18}F-FDG PET and DWI Datasets for Predicting Therapy Response of Soft-Tissue Sarcomas Under Neoadjuvant Isolated Limb Perfusion

Michal Chodyla[1], Aydin Demircioglu[1], Benedikt M. Schaarschmidt[1], Stefanie Bertram[2], Nils Martin Bruckmann[3], Jennifer Haferkamp[1], Yan Li[1], Sebastian Bauer[4], Lars Podleska[5], Christoph Rischpler[6], Michael Forsting[1], Ken Herrmann[6], Lale Umutlu[1], and Johannes Grueneisen[1]

[1]Department of Diagnostic and Interventional Radiology, University Hospital Essen, University of Duisburg–Essen, Essen, Germany; [2]Institute of Pathology, University Hospital Essen, University of Duisburg–Essen, Essen, Germany; [3]Department of Diagnostic and Interventional Radiology, University Hospital Dusseldorf, University of Dusseldorf, Dusseldorf, Germany; [4]Sarcoma Center, Western German Cancer Center, University of Duisburg–Essen, Essen, Germany; [5]Sarcoma Surgery Division, Department of General, Visceral, and Transplantation Surgery, University Hospital Essen, University of Duisburg–Essen, Essen, Germany; and [6]Department of Nuclear Medicine, University Hospital Essen, University of Duisburg–Essen, Essen, Germany

Our purpose was to evaluate and compare the clinical utility of simultaneously obtained quantitative ^{18}F-FDG PET and diffusion-weighted MRI datasets for predicting the histopathologic response of soft-tissue sarcoma (STS) to neoadjuvant isolated limb perfusion (ILP). **Methods:** In total, 37 patients with a confirmed STS of the extremities underwent ^{18}F-FDG PET/MRI before and after ILP with melphalan and tumor necrosis factor-α. For each patient, the maximum tumor size, metabolic activity (SUV), and diffusion restriction (apparent diffusion coefficient, ADC) were determined in pre- and posttherapeutic examinations, and percentage changes during treatment were calculated. Mann–Whitney *U* testing and receiver-operating-characteristic analysis were used to compare the results of the different quantitative parameters to predict the histopathologic response to therapy. Results from histopathologic analysis after tumor resection served as the reference standard, and patients were defined as responders or nonresponders based on the grading scale by Salzer-Kuntschik. **Results:** Histopathologic analysis categorized 22 (59%) patients as responders (grades I–III) and 15 (41%) as nonresponders (grades IV–VI). Under treatment, tumors in responders showed a mean reduction in size (−9.7%) and metabolic activity (SUV_{peak}, −51.9%; SUV_{mean}, −43.8%), as well as an increase of the ADC values (ADC_{min}, +29.4%; ADC_{mean}, +32.8%). The percentage changes in nonresponders were −6.2% in tumor size, −17.3% in SUV_{peak}, −13.9% in SUV_{mean}, +15.3% in ADC_{min}, and +14.6% in ADC_{mean}. Changes in SUV and ADC_{mean} significantly differed between responders and nonresponders (<0.01), whereas differences in tumor size and ADC_{min} did not (>0.05). The corresponding AUCs were 0.63 for tumor size, 0.87 for SUV_{peak}, 0.82 for SUV_{mean}, 0.63 for ADC_{min}, 0.84 for ADC_{mean}, and 0.89 for ratio of ADC_{mean} to SUV_{peak}. **Conclusion:** PET- and MRI-derived quantitative parameters (SUV and ADC_{mean}) and their combination performed well in predicting the histopathologic therapy response of STS to neoadjuvant ILP. Therefore, integrated PET/MRI could serve as a valuable tool for pretherapeutic assessment as well as monitoring of neoadjuvant treatment strategies of STS.

Received Apr. 26, 2020; revision accepted Jun. 26, 2020.
For correspondence or reprints contact: Johannes Grueneisen, Department of Diagnostic and Interventional Radiology, University Hospital Essen, Hufelandstrasse 55, 45147 Essen, Germany.
E-mail: johannes.grueneisen@uk-essen.de
Published online Jul. 31, 2020.

Key Words: soft-tissue sarcoma; isolated limb perfusion; ^{18}F-FDG PET; DWI; therapy response prediction

J Nucl Med 2021; 62:348–353
DOI: 10.2967/jnumed.120.248260

Limb salvage is a major goal for patients with diagnosed soft-tissue sarcoma (STS) of the extremities. Therefore, neoadjuvant treatment is frequently applied for primary nonresectable tumors to achieve local tumor control and complete tumor resection (*1*). It has been demonstrated that a good clinical outcome, in terms of high limb salvage rates and fewer locoregional tumor recurrences, requires a good histopathologic tumor response to neoadjuvant therapy and is equivalent to limb amputation, considering patients' survival (*2,3*).

Hyperthermic isolated limb perfusion (ILP) with tumor necrosis factor-α and melphalan is an efficient preoperative treatment for STS to ensure local disease regression (*4,5*). This technique enables the administration of high regional drug concentrations with limb salvage rates above 70% (*6*). However, there is generally a need to reliably assess treatment success before subsequent tumor resection, in order to consider further therapeutic interventions if the initial treatment was not sufficient.

In clinical routine, size- and morphology-based therapy monitoring is commonly applied yet has not been shown appropriate for reliable response evaluation of STS (*7*). Some previous studies have already investigated the use of ^{18}F-FDG PET data for response assessment of STS and reported better results than for size and volumetric tumor measurements (*8–10*). Besides morphologic and metabolic imaging datasets, PET/MRI scanners allow for the simultaneous acquisition of further functional imaging parameters. Diffusion-weighted imaging (DWI) has been widely established in oncologic imaging and provides information about the composition and structure of biologic tissues (*11,12*). It has been shown that the DWI-derived apparent diffusion coefficient (ADC) can be applied as a quantitative imaging biomarker for predicting and monitoring therapeutic effects on solid tumors (*13,14*). Accordingly,

the current study evaluated and directly compared the potential of PET/MRI-based quantitative imaging parameters, as well as their combination, for assessing the response of STS to neoadjuvant ILP.

MATERIALS AND METHODS

Patients

The institutional review board approved this prospective study, and all patients gave written informed consent before each examination. In total, 37 patients (mean age, 51.8 ± 12.5 y) with primary ($n = 31$) or recurrent ($n = 6$) STS were included. All patients were enrolled for an ^{18}F-FDG PET/MRI examination within 1 wk before the treatment procedure, as well as for a second scan after neoadjuvant ILP (mean delay, 44.3 ± 8.6 d) and before subsequent tumor resection. Table 1 gives an overview of the different STS subtypes included in this study.

ILP

Neoadjuvant ILP was performed under general anesthesia and mild hyperthermia of 39°. For tumors of the upper limb, vascular access via a brachial or axillary approach was chosen, and for STS of the lower limb, a femoral or iliac approach was used. As a first step, recombinant human tumor necrosis factor-α (Beromun; Boehringer-Ingelheim) was applied and adjusted to 0.25 mg/L of perfused-tissue volume; in addition, with a delay of 15 min, melphalan (L-phenylalanine mustard) was administered at a concentration of 11 mg/L of limb volume for legs and 13 mg/L for arms. Continuous monitoring for leakage was performed using nuclear medicine testing with radiolabeled serum (^{111}In).

PET/MRI

All PET/MRI examinations were acquired on a 3-T Biograph mMR scanner (Siemens Healthineers) with the patient supine and with a delay of 60 min after a body weight–adapted dosage of ^{18}F-FDG had been administered intravenously (mean activity, 245 ± 33 MBq [first scan] and 237 ± 35 MBq [second scan]). PET/MRI datasets were obtained at 1–2 bed positions covering the entire tumor volume, with a 10-min PET acquisition time per bed position.

Images were subsequently reconstructed using iterative ordered-subset expectation maximization, with 3 iterations and 21 subsets, a gaussian filter of 4 mm in full width at half maximum, and a 344 × 344 image matrix. PET images were automatically attenuation-corrected on the basis of a 4-compartment-model attenuation map calculated from fat-only and water-only datasets, as obtained by Dixon-based sequences, facilitating a segmentation into background, lung, fat, and soft tissue. MRI data were acquired simultaneously with PET data using dedicated mMR body phased-array coils and mMR spine coils and the following sequence protocol: a coronal 3-dimensional volume-interpolated breath-hold sequence, a coronal short-tau inversion-recovery sequence, a transversal T1-weighted turbo spin-echo sequence, a transversal T2-weighted turbo spin-echo sequence, a transversal diffusion-weighted echo-planar imaging sequence, and a fat-saturated transversal 3-dimensional volume-interpolated breath-hold sequence for dynamic imaging. An intravenous contrast agent (gadobutrol, 0.1 mmol/kg of body weight; Bayer Healthcare) was administered, and 3 repetitive scans were acquired at a delay of 25, 54, and 86 s. Additionally, transversal and coronal postcontrast fat-saturated T1-weighted turbo spin-echo sequences were acquired. Detailed information about the MRI sequence parameters are given in Supplemental Table 1 (supplemental materials are available at http://jnm.snmjournals.org).

Data Analysis

Two physicians with 7 and 8 y of experience in reading MR and hybrid images analyzed the acquired PET/MRI datasets in consensus, using dedicated viewing software for hybrid imaging (Syngo.via B30; Siemens Healthineers). Both readers knew the diagnosis and the treatment procedure but they were blinded regarding the results of histopathologic analysis after subsequent tumor resection.

In a first step, the readers were instructed to determine the maximum tumor diameter on contrast-enhanced fat-saturated T1-weighted MR images from pre- and posttherapeutic PET/MRI examinations. For the evaluation of diffusion restriction of the STS, an ADC map was generated by the scanner software (Syngo MR B18P; Siemens Healthineers) using 3 different b-values (0, 500, and 1,000 s/mm^2). Tumor lesions were identified on diffusion-weighted sequences, and a polygonal region of interest was manually drawn on every slice of the corresponding ADC map, covering the entire lesion. After visual confirmation of correct placement, ADC values were determined. Furthermore, measurements of the metabolic activity of the STS manifestations were performed. Therefore, a polygonal region of interest was manually drawn on every slice of the PET/MR images, covering the entire tumor volume, and SUV_{peak} (average SUV within a spheric 1 cm^3 volume of interest around the hottest point in the tumor) and SUV_{mean} were obtained.

Reference Standard

For the determination of treatment response or nonresponse of STS to neoadjuvant ILP, histopathologic analysis of surgical specimen after subsequent tumor resection served as the reference standard. Microscopic analysis was performed on hematoxylin- and eosin-stained slides, and in each case tumor regression was assessed by light microscopy according to the grading scale of Salzer-Kuntschik et al. (*15*). On the basis of the percentage of viable tumor, histopathologic findings were subdivided into 6 grades (grade I, no vital tumor; grade II, single vital tumor cell or 1 cluster/5 mm; grade III, <10% vital tumor; grade IV, 10%–50% vital tumor; grade V, >50% vital tumor; and grade VI, no therapeutic effect). In accordance with previous

TABLE 1
Histologic Subtypes of STSs

Subtype	Patients (*n*)
Undifferentiated pleomorphic sarcoma	9
Synovial sarcoma	9
Myxofibrosarcoma	6
Liposarcoma	6
Undifferentiated spindle cell sarcoma	3
Leiomyosarcoma	2
Epitheloid sarcoma	1
Malignant peripheral nerve sheath tumor	1
Total	37

TABLE 2
Regression Grades According to 6-Grade Scale of Salzer-Kuntschik et al. (*15*)

Grade	Patients (*n*)
I	5
II	5
III	12
IV	6
V	8
VI	1
Total	37

TABLE 3
Results of Quantitative Image Analysis for PET- and MRI-Derived Parameters

Parameter	Responder			Nonresponder			*P*
	Pretherapeutic	Posttherapeutic	Percentage change	Pretherapeutic	Posttherapeutic	Percentage change	
Size	92.6 ± 62.0	85.7 ± 62.6	−9.7 ± 9.8	114.6 ± 59.5	108.7 ± 61.8	−6.2 ± 9.0	0.191
SUV_{mean}	5.8 ± 3.3	2.5 ± 1.2	−43.8 ± 35.6	2.9 ± 1.3	2.5 ± 1.5	−13.9 ± 21.3	0.001
SUV_{peak}	8.6 ± 4.6	3.4 ± 1.8	−51.9 ± 26.6	4.3 ± 3.2	3.7 ± 3.2	−17.3 ± 17.9	<0.001
ADC_{min}	568.3 ± 156.0	708.7 ± 173.6	+29.4 ± 35.2	652.1 ± 186.0	737.0 ± 220.4	+15.3 ± 29.1	0.202
ADC_{mean}	1279.6 ± 198.3	1678.7 ± 196.6	+32.8 ± 17.2	1412.1 ± 277.9	1603.2 ± 277.1	+14.6 ± 10.2	<0.001
ADC_{mean}/SUV_{peak} ratio	225.8 ± 189.4	628.1 ± 298.2	+266.2 ± 208.9	452.7 ± 226.2	657.1 ± 323.4	+43.2 ± 26.6	<0.001

Data are mean ± SD.

publications, stages I–III were categorized as histopathologic responders and stages IV–VI as nonresponders (*7,16*).

Statistical Analysis

Statistical analysis was performed using the R software environment for statistical computing and graphics (version 3.6.1). Quantitative PET- and MRI-derived parameters and their percentage changes under therapy are presented as mean values ± SDs. In addition, for each tumor the ratio of ADC_{mean} to SUV_{peak} in pre- and posttherapeutic PET/MRI examinations, as well as their percentage changes under treatment, were calculated. Mann–Whitney *U* testing assessed for significant differences in results between responders and nonresponders. *P* values of less than 0.05 were considered statistically significant. Receiver-operating-characteristic analysis was performed, and areas under the curve (AUCs) and optimal thresholds were calculated for the quantitative parameters to predict response to ILP. For statistical comparison of different AUCs, a bootstrap test with 2,000 replicates was used.

RESULTS

Patients

All patients completed the pre- and posttherapeutic PET/MRI examinations without any relevant side effects. Histopathologic analysis after tumor resection categorized 22 (59%) patients as responders and 15 (41%) as nonresponders. The tumor grades and histologic findings are shown in Table 2 and Supplemental Table 2.

Quantitative Image Analysis

Table 3 shows the calculated mean values and percentage changes of the different PET- and MR-derived quantitative imaging parameters for histopathologic therapy responders and nonresponders. The responder group revealed a significant and stronger decrease of the SUV_{mean} ($P < 0.001$), SUV_{peak} ($P < 0.001$), and the ADC_{mean}/SUV_{peak} ratio ($P < 0.001$), as well as a stronger increase of the ADC_{mean} ($P < 0.001$) (Figs. 1 and 2), when compared with nonresponders. On the other hand, differences of the calculated mean values for tumor size ($P = 0.191$) and the ADC_{min} ($P = 0.202$) did not reach significant level between histopathologic therapy responders and nonresponders.

According to the receiver-operating-characteristic analysis for prediction of histopathologic treatment response, the AUC for SUV_{peak} was slightly and insignificantly higher than those for ADC_{mean} and SUV_{mean} but differed significantly from those for tumor size and ADC_{min} (Table 4; Fig. 3). In addition, a significantly higher AUC value was obtained for the ADC_{mean}, when compared with the ADC_{min}. Moreover, the ratio of the ^{18}F-FDG PET– and DWI-derived imaging parameters with the best predictive values was calculated (ADC_{mean}/SUV_{peak}) and had the highest AUC among the different variables, but differences from the results for SUV_{peak}, ADC_{mean}, and SUV_{mean} were not significant.

The optimal thresholds for percentage changes in quantitative variables to discriminate between a histopathologic therapy response and a nonresponse were −4.11% for tumor size, −34.44% for SUV_{mean}, −43.82% for SUV_{peak}, 25.39% for ADC_{min}, 20.41% for ADC_{mean}, and 98.09% for ADC_{mean}/SUV_{peak} ratio.

DISCUSSION

Hyperthermic ILP with tumor necrosis factor-α and melphalan is a highly effective neoadjuvant treatment to achieve local tumor control and limb-preserving surgery in locally advanced STS of the extremities (*4,5*). A good histopathologic tumor response, defined as less than 10% of viable tumor cells remaining after therapy, is associated with a reduced number of local recurrences and increased limb salvage rates (*2,7,16*). In the present study, histopathologic analysis revealed more than 90% tumor regression in 22 of 37 (59%) patients after ILP. A potential explanation for this moderate response rate is the inclusion of a heterogeneous study population comprising patients with both primary and recurrent sarcoma manifestations. Furthermore, it has been shown that

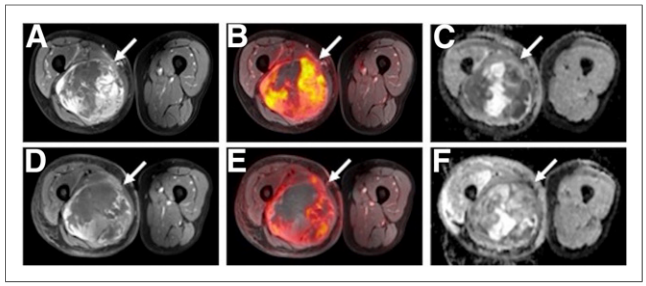

FIGURE 1. Pretherapeutic (A–C) and posttherapeutic (D–F) images of 63-y-old patient with STS (myxofibrosarcoma; arrows) of right upper leg. Tumor size remains substantially stable after treatment (size: −1.1%; A and C, MRI), whereas tumor reveals significant changes in ^{18}F-FDG uptake (SUV_{peak}: −60.4%; B and D, PET/MRI) and diffusion restriction (ADC_{mean}: +37.4%; C and F, ADC map). Histopathologic analysis after surgical resection revealed grade 3 regression (responder).

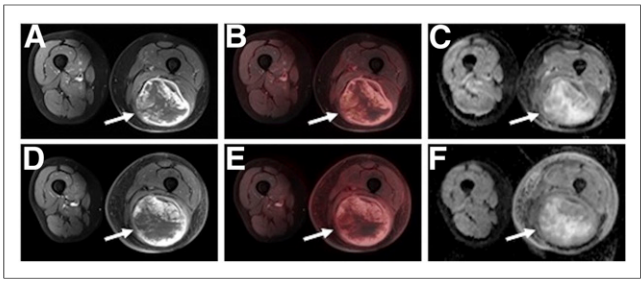

FIGURE 2. Images of 56-y-old patient with STS (leiomyosarcoma; arrows) of left upper leg. Tumor does not show relevant change in size (+5.3%; A and C, MRI), metabolic activity (SUV_{peak}: −7.7%, B and E, PET/MRI), or diffusion restriction (ADC_{mean}: −5.1%, C and F, ADC map) on pretherapeutic (A–C) and posttherapeutic (D–F) PET/MR images and was classified as nonresponder (regression grade 5) after surgical resection.

different subtypes of STS have variable response rates to ILP (*3*). In a study by Grabellus et al., synovial sarcoma, spindle cell sarcoma, liposarcoma, epitheloid sarcoma, and malignant peripheral nerve sheath tumors, which account for more than 50% of the included entities in the present study, revealed only moderate tumor regression (*3*). Therefore, presurgical evaluation of initial treatment success is important in considering further therapies when neoadjuvant treatment is not sufficient.

MRI is the recommended and most commonly applied imaging modality for presurgical planning and treatment monitoring of STS of the extremities (*17,18*). However, previous studies demonstrated that morphologic criteria, such as RECIST, do not reliably assess the response of STS to neoadjuvant therapy (*7,19*). Likewise, our results revealed only a weak correlation between a solely size-based response evaluation and therapy-induced histopathologic changes. STS commonly show structural changes (in terms of the development of fibrosis, granulation tissue, and necrosis as an initial histologic therapeutic effect), which frequently precede noticeable changes in tumor size (*20*).

Moreover, the introduction of DWI as an additional functional parameter to morphologic MR imaging has been demonstrated to facilitate significant improvements in tumor detection and noninvasive characterization of biologic tissues (*21–23*). On the basis of the restricted motion of water molecules within cancer lesions, caused by higher cell densities, DWI-derived ADC values have been recognized as valuable quantitative parameters for the assessment of tissue compositions and can be applied as an imaging biomarker for predicting and monitoring therapeutic effects of solid tumors (*24,25*). In the present study, significant differences were found in the percentage change in ADC_{mean} between responders and nonresponders, and this parameter performed well, with a high AUC (0.84) for predicting histopathologic response to ILP. The ADC_{mean} enables the quantification of potential changes of the mean tumor cellularity under treatment, covering the entire volume of the STS manifestation. Hence, a therapy-induced loss of viable tumor cells, accompanied with the induction of tumor necrosis, leads to a measurable increase of the ADC_{mean} value, based on the higher fluid amount and the decrease of solid tumor parts. Accordingly, the ADC_{mean} value provides valuable information about alterations in tissue structure without invasive tissue sampling—alterations that are also reflected by the regression grading scale of Salzer-Kuntschik (*15*). Hayashida et al. reported comparable results, showing a significantly stronger increase in ADC_{mean} for responders than nonresponders, whereas no differences in the volumetric measurements of the sarcomas were found between the 2 groups under treatment (*26*). Baunin et al. demonstrated that the ADC values increased significantly stronger in sarcoma patients with good pathologic response, even at a midcourse DW-MRI scan under chemotherapy, when compared with patients with poor response (*27*). In addition, Soldatos et al. showed that adding functional MRI sequences (e.g., DWI datasets) to a conventional MRI protocol increases the sensitivity for defining treatment response of STS (*28*). Surprisingly, our results revealed only a weak association between the ADC_{min} and therapy-induced histopathologic changes. An explanation may be the structural heterogeneity of these frequently large tumors, whereby even small remaining solid tumor parts with restricted diffusivity have a relevant influence on this parameter. In addition, the specific compositions of the different histologic sarcoma subtypes, as well as the occurrence of blood products due to hemorrhage (e.g., an increased fluid amount, clots, etc.) after therapy, might have affected ADC measurements.

Numerous publications have already demonstrated the high performance of ^{18}F-FDG PET data for staging tumors and monitoring the effect of therapy on various cancers (*29–31*). Some studies focusing on the evaluation of sarcoma patients showed that ^{18}F-FDG PET–based metabolic information can help to predict disease progression and survival in patients undergoing neoadjuvant systemic therapy (*32–34*). In addition, a few previous articles reported that therapeutic response was more accurately assessed by ^{18}F-FDG PET data quantifications than by tumor size measurements (*8–10,35*). In our study, SUV_{peak} provided the best results

TABLE 4
Results of Receiver-Operating-Characteristic Analysis

Parameter	Size	SUV_{mean}	SUV_{peak}	ADC_{min}	ADC_{mean}	ADC_{mean}/SUV_{peak} ratio
Size	0.630*	0.150	0.036†	0.981	0.097	0.020†
SUV_{mean}		0.815*	0.295	0.117	0.803	0.151
SUV_{peak}			0.871*	0.019†	0.690	0.150
ADC_{min}				0.627*	0.024†	0.007†
ADC_{mean}					0.839*	0.463
ADC_{mean}/SUV_{peak} ratio						0.894*

*AUC.
†*P* value indicating statistical difference between quantitative variables.

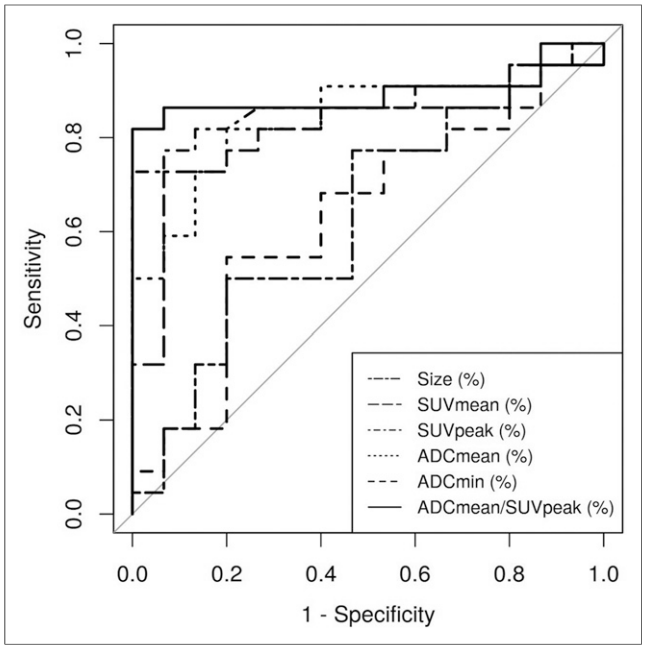

FIGURE 3. Receiver-operating-characteristic curves of quantitative variables for prediction of histopathologic response to ILP.

among the different PET- and MRI-derived parameters, with a significantly higher AUC (0.87) than was obtained for ADC_{min} (0.63) or tumor size (0.63). On the other hand, AUCs for SUV_{peak}, SUV_{mean}, and ADC_{mean} differed only slightly and not significantly from one another. Byun et al. reported a significant inverse correlation between percentage change in SUV and percentage change in ADC in osteosarcomas under neoadjuvant chemotherapy (*36*). In their work, the combination of SUV and ADC was superior (0.85) to SUV (0.77) or ADC (0.73) alone for predicting a good histologic response (*36*). In concordance with these findings, the ADC_{mean}/SUV_{peak} ratio used in the present study tended to evaluate treatment response more reliably, but the results did not differ significantly from those for either of the 2 quantitative parameters alone. Considering the complementary information provided by the 2 parameters, a combined analysis may be a more sustainable way to assess histologic response.

Our study was not without limitations. In view of the limited number of patients, the results have to be considered preliminary and need to be verified in larger patient cohorts. Data analysis was performed in a consensus reading; hence, no specific data on interrater reliability could be collected. The fact that patients with primary tumors, recurrent sarcoma, and different histopathologic subtypes were included might have affected the results. As a standard procedure, histopathologic analysis was performed on certain representative slices of tumor; however, the volumetric measurements of the quantitative parameters did not allow for a precise correlation between tissue histology and MRI data.

CONCLUSION

Our study results demonstrate a good performance of ^{18}F-FDG PET and MR-derived quantitative imaging parameters (SUVs and ADC_{mean}) for the prediction of histopathologic therapy response of STS under neoadjuvant ILP. Especially, the combined and complementary information derived from these imaging features, reflecting different aspects of the underlying tumor biology, may provide more reliable evaluation of treatment effects of STS manifestations, when compared to sole morphologic assessment. Therefore, integrated PET/MRI could serve as a valuable diagnostic tool for pretherapeutic and presurgical assessment as well as monitoring of neoadjuvant therapeutic strategies of STS.

DISCLOSURE

No potential conflict of interest relevant to this article was reported.

KEY POINTS

QUESTION: Do quantitative parameters derived from ^{18}F-FDG PET and MRI reliably predict the response of STS to neoadjuvant ILP?

PERTINENT FINDINGS: Mean SUV_{peak}, SUV_{mean}, and ADC_{mean}/SUV_{peak} ratio revealed a significantly stronger decrease, and ADC_{mean} a stronger increase, in responders than in nonresponders, whereas no significant differences in tumor size or ADC_{min} were found between the 2 groups. Receiver-operating-characteristic analysis revealed high AUC values for the SUV_{peak}, the ADC_{mean}, and the ratio ADC_{mean}/SUV_{peak} to predict histopathologic treatment that differed significantly from the AUCs for tumor size or ADC_{min}.

IMPLICATIONS FOR PATIENT CARE: ^{18}F-FDG PET/MRI data may be valuable when added to diagnostic algorithms that evaluate and predict the response of STS to neoadjuvant therapy.

REFERENCES

1. Hohenberger P, Wysocki WM. Neoadjuvant treatment of locally advanced soft tissue sarcoma of the limbs: which treatment to choose? *Oncologist.* 2008;13:175–186.
2. Williard WC, Hajdu SI, Casper ES, Brennan MF. Comparison of amputation with limb-sparing operations for adult soft tissue sarcoma of the extremity. *Ann Surg.* 1992;215:269–275.
3. Grabellus F, Kraft C, Sheu-Grabellus SY, et al. Tumor vascularization and histopathologic regression of soft tissue sarcomas treated with isolated limb perfusion with TNF-alpha and melphalan. *J Surg Oncol.* 2011;103:371–379.
4. Eggermont AM, Schraffordt Koops H, Klausner JM, et al. Isolated limb perfusion with tumor necrosis factor and melphalan for limb salvage in 186 patients with locally advanced soft tissue extremity sarcomas: the cumulative multicenter European experience. *Ann Surg.* 1996;224:756–764.
5. Neuwirth MG, Song Y, Sinnamon AJ, Fraker DL, Zager JS, Karakousis GC. Isolated limb perfusion and infusion for extremity soft tissue sarcoma: a contemporary systematic review and meta-analysis. *Ann Surg Oncol.* 2017;24:3803–3810.
6. Verhoef C, de Wilt JH, Grunhagen DJ, van Geel AN, ten Hagen TL, Eggermont AM. Isolated limb perfusion with melphalan and TNF-alpha in the treatment of extremity sarcoma. *Curr Treat Options Oncol.* 2007;8:417–427.
7. Grabellus F, Stylianou E, Umutlu L, et al. Size-based clinical response evaluation is insufficient to assess clinical response of sarcomas treated with isolated limb perfusion with TNF-alpha and melphalan. *Ann Surg Oncol.* 2012;19:3375–3385.
8. Evilevitch V, Weber WA, Tap WD, et al. Reduction of glucose metabolic activity is more accurate than change in size at predicting histopathologic response to neoadjuvant therapy in high-grade soft-tissue sarcomas. *Clin Cancer Res.* 2008;14:715–720.
9. Denecke T, Hundsdorfer P, Misch D, et al. Assessment of histological response of paediatric bone sarcomas using FDG PET in comparison to morphological volume measurement and standardized MRI parameters. *Eur J Nucl Med Mol Imaging.* 2010;37:1842–1853.
10. Grueneisen J, Schaarschmidt B, Demircioglu A, et al. ^{18}F-FDG PET/MRI for therapy response assessment of isolated limb perfusion in patients with soft-tissue sarcomas. *J Nucl Med.* 2019;60:1537–1542.
11. Koh DM, Collins DJ. Diffusion-weighted MRI in the body: applications and challenges in oncology. *AJR.* 2007;188:1622–1635.

12. Bonekamp S, Corona-Villalobos CP, Kamel IR. Oncologic applications of diffusion-weighted MRI in the body. *J Magn Reson Imaging.* 2012;35:257–279.
13. Padhani AR, Koh DM. Diffusion MR imaging for monitoring of treatment response. *Magn Reson Imaging Clin N Am.* 2011;19:181–209.
14. Schreuder SM, Lensing R, Stoker J, Bipat S. Monitoring treatment response in patients undergoing chemoradiotherapy for locally advanced uterine cervical cancer by additional diffusion-weighted imaging: a systematic review. *J Magn Reson Imaging.* 2015;42:572–594.
15. Salzer-Kuntschik M, Delling G, Beron G, Sigmund R. Morphological grades of regression in osteosarcoma after polychemotherapy: study COSS 80. *J Cancer Res Clin Oncol.* 1983;106(suppl):21–24.
16. Stacchiotti S, Collini P, Messina A, et al. High-grade soft-tissue sarcomas: tumor response assessment—pilot study to assess the correlation between radiologic and pathologic response by using RECIST and Choi criteria. *Radiology.* 2009;251:447–456.
17. De Schepper AM, De Beuckeleer L, Vandevenne J, Somville J. Magnetic resonance imaging of soft tissue tumors. *Eur Radiol.* 2000;10:213–223.
18. Noebauer-Huhmann IM, Weber MA, Lalam RK, et al. Soft tissue tumors in adults: ESSR-approved guidelines for diagnostic imaging. *Semin Musculoskelet Radiol.* 2015;19:475–482.
19. Canter RJ, Martinez SR, Tamurian RM, et al. Radiographic and histologic response to neoadjuvant radiotherapy in patients with soft tissue sarcoma. *Ann Surg Oncol.* 2010;17:2578–2584.
20. DeLaney TF, Spiro IJ, Suit HD, et al. Neoadjuvant chemotherapy and radiotherapy for large extremity soft-tissue sarcomas. *Int J Radiat Oncol Biol Phys.* 2003;56:1117–1127.
21. Low RN, Sebrechts CP, Barone RM, Muller W. Diffusion-weighted MRI of peritoneal tumors: comparison with conventional MRI and surgical and histopathologic findings—a feasibility study. *AJR.* 2009;193:461–470.
22. Hong JH, Jee WH, Jung CK, Jung JY, Shin SH, Chung YG. Soft tissue sarcoma: adding diffusion-weighted imaging improves MR imaging evaluation of tumor margin infiltration. *Eur Radiol.* 2019;29:2589–2597.
23. Pickles MD, Gibbs P, Sreenivas M, Turnbull LW. Diffusion-weighted imaging of normal and malignant prostate tissue at 3.0T. *J Magn Reson Imaging.* 2006;23:130–134.
24. Liu Y, Bai R, Sun H, Liu H, Zhao X, Li Y. Diffusion-weighted imaging in predicting and monitoring the response of uterine cervical cancer to combined chemoradiation. *Clin Radiol.* 2009;64:1067–1074.
25. Wang L, Liu L, Han C, et al. The diffusion-weighted magnetic resonance imaging (DWI) predicts the early response of esophageal squamous cell carcinoma to concurrent chemoradiotherapy. *Radiother Oncol.* 2016;121:246–251.
26. Hayashida Y, Yakushiji T, Awai K, et al. Monitoring therapeutic responses of primary bone tumors by diffusion-weighted image: initial results. *Eur Radiol.* 2006;16:2637–2643.
27. Baunin C, Schmidt G, Baumstarck K, et al. Value of diffusion-weighted images in differentiating mid-course responders to chemotherapy for osteosarcoma compared to the histological response: preliminary results. *Skeletal Radiol.* 2012;41:1141–1149.
28. Soldatos T, Ahlawat S, Montgomery E, Chalian M, Jacobs MA, Fayad LM. Multiparametric assessment of treatment response in high-grade soft-tissue sarcomas with anatomic and functional MR imaging sequences. *Radiology.* 2016;278:831–840.
29. Usmanij EA, Natroshvili T, Timmer-Bonte JNH, et al. The predictive value of early in-treatment ^{18}F-FDG PET/CT response to chemotherapy in combination with bevacizumab in advanced nonsquamous non-small cell lung cancer. *J Nucl Med.* 2017;58:1243–1248.
30. Antoch G, Stattaus J, Nemat AT, et al. Non-small cell lung cancer: dual-modality PET/CT in preoperative staging. *Radiology.* 2003;229:526–533.
31. Benz MR, Evilevitch V, Allen-Auerbach MS, et al. Treatment monitoring by ^{18}F-FDG PET/CT in patients with sarcomas: interobserver variability of quantitative parameters in treatment-induced changes in histopathologically responding and nonresponding tumors. *J Nucl Med.* 2008;49:1038–1046.
32. Fendler WP, Lehmann M, Todica A, et al. PET response criteria in solid tumors predicts progression-free survival and time to local or distant progression after chemotherapy with regional hyperthermia for soft-tissue sarcoma. *J Nucl Med.* 2015;56:530–537.
33. Eary JF, O'Sullivan F, Powitan Y, et al. Sarcoma tumor FDG uptake measured by PET and patient outcome: a retrospective analysis. *Eur J Nucl Med Mol Imaging.* 2002;29:1149–1154.
34. Schuetze SM, Rubin BP, Vernon C, et al. Use of positron emission tomography in localized extremity soft tissue sarcoma treated with neoadjuvant chemotherapy. *Cancer.* 2005;103:339–348.
35. Herrmann K, Benz MR, Czernin J, et al. ^{18}F-FDG-PET/CT imaging as an early survival predictor in patients with primary high-grade soft tissue sarcomas undergoing neoadjuvant therapy. *Clin Cancer Res.* 2012;18:2024–2031.
36. Byun BH, Kong CB, Lim I, et al. Combination of ^{18}F-FDG PET/CT and diffusion-weighted MR imaging as a predictor of histologic response to neoadjuvant chemotherapy: preliminary results in osteosarcoma. *J Nucl Med.* 2013;54:1053–1059.